Applied Catalysis B: Environmental 187 (2016) 83–89

Contents lists available at ScienceDirect

Applied Catalysis B: Environmental

journal homepage: www.elsevier.com/locate/apcatb

Accelerated methylene blue (MB) degradation by Fenton reagent exposed to UV or VUV/UV light in an innovative micro photo-reactor

Mengkai Li [a,b], Zhimin Qiang [a], Cesar Pulgarin [b], John Kiwi [b,*]

[a] Key Laboratory of Drinking Water Science and Technology, Research Center for Eco-Environmental Sciences, Chinese Academy of Sciences, 18 Shuang-qing Road, Beijing 100085, China
[b] Ecole Polytechnique Fédérale de Lausanne, EPFL-SB-ISIC-GPAO, Station 6, CH-1015 Lausanne, Switzerland

ARTICLE INFO

Article history:
Received 5 November 2015
Received in revised form 4 January 2016
Accepted 9 January 2016
Available online 13 January 2016

Keywords:
Vacuum-UV (VUV)
Photo-Fenton
Micro photo-reactor
Methylene blue
Oxidative radicals
Reaction mechanism

ABSTRACT

This study presents the accelerated discoloration/degradation of methylene blue (MB) in solution by Fenton reagent under exposure to ultraviolet (UV) or Vacuum-UV/UV (VUV/UV) light in an innovative micro photo-reactor. The MB degradation was kinetically faster when using VUV/UV light at 254/185 nm compared to UV-irradiation at 254 nm. Oxidative radicals produced by the photo-Fenton process were identified with appropriate scavengers. The addition of benzoquinone (BQ) at millimolar (mM) concentrations to MB solutions precluded completely the MB photo-induced bleaching, while *tert*-butanol hindered to a lesser extent the MB degradation suggesting that $HO_2^{\bullet}$ was the predominant intermediate leading to MB degradation. The VUV/UV micro photo-reactor comprised mercury resonance lines at 185 and 254 nm. The photon percentages absorbed by water were estimated to be 16.8% at 254 nm and 78.3% at 185 nm by water, while those absorbed by H_2O_2 were 0.9% and 2.2%, correspondingly. The solution parameters affecting the features of MB degradation, such as MB, Fe, and H_2O_2 concentrations, were explored and reaction mechanism was proposed. The lifetimes of $^{\bullet}OH$ and $HO_2^{\bullet}$ were estimated to be 2 ns and 0.38 s under an optimized solution with 0.016 mM MB, 0.147 mM H_2O_2 and 0.05 mM Fe^{3+}. Moreover, an estimation of the mean free paths of these radicals in solution provided the evidence that it was the radical lifetimes and mean-free paths, not their oxidation potentials that controlled the MB degradation kinetics. This study shows the potential of this VUV/UV assistant photo-Fenton process for the degradation of diluted organic compounds in aqueous solution.

1. Introduction

In recent decades, several advanced oxidation processes (AOPs) that produce highly oxidative radicals such as $^{\bullet}OH$, $^{\bullet}OH$, $Cl^{\bullet}$ have been reported and applied in water/wastewater treatments [1–10]. The Fenton/photo-Fenton process has been widely reported for the decontamination of a large range of recalcitrant and/or non-biodegradable pollutants during the treatment of industrial wastewaters [11–16]. Photo-Fenton studies deal with the process driven by UV or visible light irradiation generating oxidative radicals from Fe^{3+}/H_2O_2 [17–22]. The main reactions are shown below. The reaction $H_2O_2 + h\nu \rightarrow 2^{\bullet}OH$ is not important due to the sub-millimolar (mM) H_2O_2 concentration used

$$Fe^{2+} + H_2O_2 \rightarrow Fe^{3+} + {}^{\bullet}OH + OH^- \; k_1 = 76\,M^{-1}\,s^{-1} \quad (1)$$

$$Fe^{3+} + H_2O_2 \rightarrow Fe^{2+} + HO_2^{\bullet} + H^+ \; k_2 = 2 \times 10^{-2}\,M^{-1}\,s^{-1} \quad (2)$$

$$Fe^{3+} + HO_2^{\bullet} \rightarrow Fe^{2+} + O_2 + H^+ \; k_3 = 10^4\,M^{-1}\,s^{-1} \quad (3)$$

$$Fe^{2+} + {}^{\bullet}OH \rightarrow Fe^{3+} + OH^- \; k_4 = 4.3 \times 10^8\,M^{-1}\,s^{-1} \quad (4)$$

$$H_2O_2 + {}^{\bullet}OH \rightarrow HO_2^{\bullet} + H_2O \; k_5 = 2.7 \times 10^7 \quad (5)$$

$$Fe^{3+}/Fe(III)(OH)^{2+} + h\nu \rightarrow Fe^{2+}/Fe(II) + {}^{\bullet}OH [12, 15] \quad (6)$$

UV-light sources in photo-reactors commonly use the 254 nm low-pressure mercury emission line with a relative high photo-electric conversion efficiency of ~30% in the UV-range [23,24]. Low-pressure mercury lamps are able to generate mercury resonance lines at 254 nm and 185 nm. The percentage of 185 nm photons varies between 8% [25] and 25% [26] depending on the lamp power and manufacturer. These lamps use synthetic quartz of high purity allowing full transparency for the mercury resonance line at 185 nm [25,26].

The VUV generates radical and ions in water as reported by several laboratories [27–30]. VUV photolysis of pure liquid water leads to radicals $^{\bullet}OH$, $HO_2^{\bullet}$, $O_2^{\bullet -}$, $H^{\bullet}$, and stable species like H_2O_2,

* Corresponding author.
E-mail address: john.kiwi@epfl.ch (J. Kiwi).

http://dx.doi.org/10.1016/j.apcatb.2016.01.014
0926-3373/

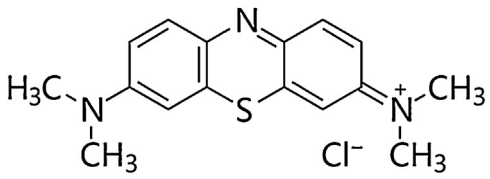

Scheme 1. (MB).

HO_2^-, O_2. In this study the kinetics of photoreactions depends on the molar absorption coefficient of water and of methylene blue (MB) in the UV and VUV region. The degradation by H_2O_2/UV of 4-chlorophenol in a slurry photocatalytic reactor has been reported and the degradation study included modeling of the photocatlytic steps [31]. The degradation of pollutants using H_2O_2/UV has been reported using some modeling [32,33].

Even though the H_2O_2/UV process presents similarities with the VUV process, there are substantial differences: a in the H_2O_2/UV process, the photolysis of H_2O_2 only generates •OH, whereas in the VUV process, photolysis of water generates •OH, H• and e_{aq}^-, which modify the observed radical reactions. VUV is able to induce homolysis and ionization of H_2O at 185 nm, as shown below in Eqs. (7) and (8) [34,35], b H_2O_2/UV direct photolysis of many organic compounds can be neglected due to their low molar absorption coefficients since they absorb light < 200 nm [3,4].

$$H_2O + h\nu(185\,nm) \rightarrow {}^{\bullet}OH + H^{\bullet} \Phi = 0.33 \quad (7)$$

$$H_2O + h(185\,nm) \rightarrow {}^{\bullet}OH + H^+ + e_{aq}^- \Phi = 0.045 \quad (8)$$

Therefore, the radicals noted by Eqs. (7) and (8) contribute to the oxidative radicals produced by the Fenton/photo-Fenton reagent shown above in Eqs. (1)–(6) leading to MB degradation. Scheme 1 shows the MB structural formula.

The sources of •OH radicals by the Fenton reagent have been already noted in Eqs. (1), (6)–(8). But H_2O_2 by itself as noted in Eqs. (7) and (8) is an additional sources of •OH-radicals. Fig. 1 shows graphically the VUV 185/254 nm mercury lines compared to the UV254 nm mercury resonance line. The molar absorption coefficients of H_2O_2 and Fe(III) increase towards shorter wavelengths molar absorption coefficients of H_2O_2 are to low to absorb a significant amount of VUV/UV and UV light at the low molarities used in the photo-reactor. Work of our own group reported Fe-transitions in solution the microsecond region, depending on the

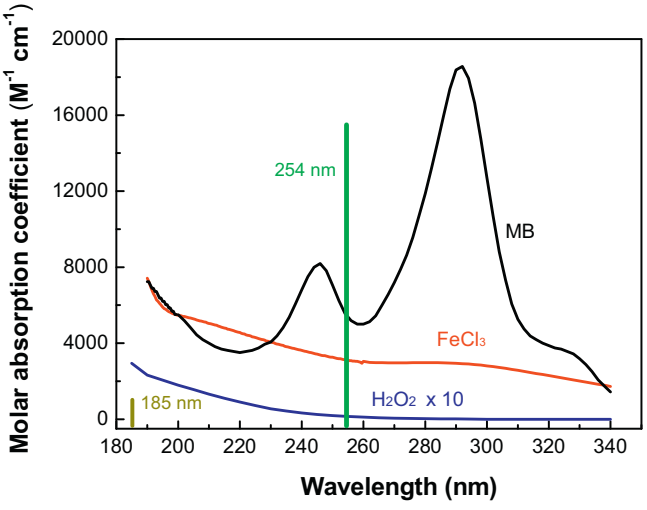

Fig. 1. The absorption spectra of H_2O_2, $FeCl_3$, and MB and the mercury resonance lines at 254 nm and 185 nm of the VUV/UV low pressure mercury lamp used throughout this study.

counter-ion, pH and Fe-species concentration [17]. The Fe (d-d) transition depend on the solution parameters and have been reported to occur within the nanosecond/microsecond range [4,36].

Recently, we have reported VUV micro photo-reactor (VMPR) for bench-scale experiments, with mercury resonance lines at 185/254 nm or alternatively presenting the mercury resonance line at 254 [37]. This precludes the very low transmittance in quasi-collimated photo-reactors in air, due to the short penetration of VUV light in air of ~50 mm. To solve this problem VUV collimated photo-reactors in a N_2 atmosphere have been recently reported [38,39]. This study reports for the first time in a detailed, systematic and comprehensive way the effect of 185/254 nm mercury resonance lines and separately the effect of the 185 nm line on the photo-Fenton mediated MB degradation in solution. This allows reporting the effect due to the radical species and the MB degradation induced by water VUV photolysis in a specific way compared to the effects of the 254 nm light in photo-Fenton mediated processes. The objective of the present study is to design and test the performance of improved AOP's technologies for water and wastewater treatment.

2. Experimental

2.1. VUV/UV photo-reactor reactor

The micro VUV/UV photo-reactor (length of 300 mm) [37] with double-layers-wall as shown in Supplementary material S1 was used throughout this study. The lamp was cooled by de-ionized water flown through the volume between double-layers-wall and the lamp housing to maintain constant lamp output. The 8W cold-cathode LP-UV synthetic quartz (arc length = 200 mm, from Haining Xiashi Co., Haining, China) emitted both 185 and 254 nm UV mercury resonance lines to obtain a uniform FR spatial distribution in the axial direction. Synthetic quartz tube was used in the photo-reactor transparent to the 185/254 nm light. A Ti-doped silica tube was used for the 254 nm light experiments. The inner diameter and length of both two tubes were 2 mm and 100 mm, respectively. Nearly same UV fluence rate (FR) could be obtained in the VUV/UV and UV tubes because both tubes presented a very high 254 nm transmittance. To obtain a uniform FR spatial distribution, two tubes were placed in the central region in the axial direction of the lamp avoiding the end-lamp regions (i.e., last 50 mm at each end of the lamp arc) where the FR distribution was observed not to be uniform. Nitrogen was flushed through the inner chamber of the reactor, to eliminate the air-absorption (e.g., O_2) and maximize the VUV reaching the samples.

2.2. Chemicals and analytical methods

Chemicals used for experiments were reagent grade or higher, supplied by Sigma-Aldrich or Fluka. Photo-Fenton experiments were carried out employing ferric chloride ($FeCl_3$) and hydrogen peroxide (35% by weight). The H_2O_2 concentration during this study was determined by the Titanium (IV) oxy-sulfate ($TiOSO_4$ Fluka) method described in Ref. [40].

The MB concentration was determined spectrophotochemically following the peak at 664 nm. The 1,4-benzoquinone (BQ) and *tert*-butanol (TBA)[2,3,10] were used as the superoxide $O_2^{\bullet -}$ and •OH scavengers, respectively. Milli-Q water (Millipore) was used in all experiments and analytical determinations.

2.3. Experimental procedures

The experimental set-up was stabilized for 15 min prior to the re-circulation of the 50 ml sample in the photo-reactor. The peak of

MB as monitored by a UV1800, Shimadzu Co., Japan spectrophotometer until the desired exposure fluence was reached. H_2SO_4 and NaOH were used to adjust the initial pH before the degradation runs. The UV–vis spectrophotometer was used to carry out the on line analysis of the absorbing species at pre-selected time intervals of 0.5 min. The samples were collected for further analysis (e.g., methanol) and analyzed by gas chromatography in the flame ionization detector.

Uridine (0.12 mM) [40] and methanol (0.1 mM) [41] were both used in the actinometry for the determination of the UV fluence (FUV) as a function of time. Details are described in Supplementary material S2. In the VUV/UV tube, methanol could measure the VUV (185 nm) fluence directly, since its UV photolysis (at 254 nm) was low (Supplementary material S3). Therefore, the total fluence in the VUV/UV tube was similar to the sum of FUV and FVUV, since 99% of the VUV/UV mercury emission lines in the UV region were at 254 nm and at 185 nm. Likewise, the total fluence in the UV tube was approximately equal to FUV, since the 185 nm photons were completely absorbed by the TiO_2-doped tube wall. In addition, in the VUV/UV tube, the exposed fluence ratio of UV (254 nm) to VUV (185 nm) was determined to be 9.2, which was similar to the ratio provided by the manufacturer of the low pressure (LP) mercury lamps.

3. Results and discussion

3.1. Basic considerations on photo-Fenton mediated reactions activated by UV and VUV light leading to MB degradation

Fig. 2a shows the MB degradation by VUV/UV, UV/UV photo-Fenton and UV photo-Fenton processes at an initial pH 3.3. The VUV/UV in the absence of H_2O_2 discolors the MB due to the radicals derived from the air (O_2) present [28–35]. Eqs. (7)–(8) also show that OH-radicals generated by water photolysis may also intervene in MB-degradation. The contribution of H_2O_2 will under irradiation by the 185/254 nm mercury resonance lines be higher compared to the 185 nm mercury resonance-line. But the light absorbed by H_2O_2 in the UV and VUV/UV region is too small to have an important effect on MB degradation at the very low H_2O_2 concentrations of 0.147 mM used in this study. The low molar absorption coefficients H_2O_2, low H_2O_2 concentrations and the low photonic fluence associated with both mercury resonance lines may be responsible for this. The H_2O_2 decomposition under light irradiation in the UV-region is shown by Eq. (9) [22–24].

$$H_2O_2 + h\nu \rightarrow 2^{\bullet}OH \Phi = 2.0 \quad (9)$$

Photo-Fenton UV/H_2O_2/Fe^{3+} reactions led to a complete MB degradation within about 8 min under UV light as shown Fig. 2a. The photochemical behavior of the Fe(III)-aqua hydroxy-complexes plays a determining role in the Fe-aqua complex absorption [36,42,43]. The pH and molar extinction coefficient of these Fe-aqua complexes play a determinant role in the photo-Fenton reactions mentioned before Eqs. (1)–(6). At pH above 3, the $Fe(H_2O)_6^{3+}$ is transformed into $Fe(III)OH(H_2O)_5^{2+}$, which is able to undergo ligand-to-metal-charge-transfer (LMCT). This treaction depends on the excitation wavelength and involves an inner sphere photo-induced electron transfer (LCMT) leading to Fe(II)-aqua complex and •OH radicals through the reaction [44].

$$Fe(III)OH(H_2O)_5^{2+} + H_2O + h\nu \rightarrow Fe(II)(H_2O)_6^{2+} + {}^{\bullet}OH \quad (10)$$

When H_2O_2 is added to the MB solution under UV and VUV/UV light as shown in Fig. 2a, the higher efficiency of MB degradation can be explained by the Fe(II)/Fe(III) inter-conversion due to the MB-radicals produced during the MB degradation. This leads to an increased •OH-radicai production [15,45]. The experiments

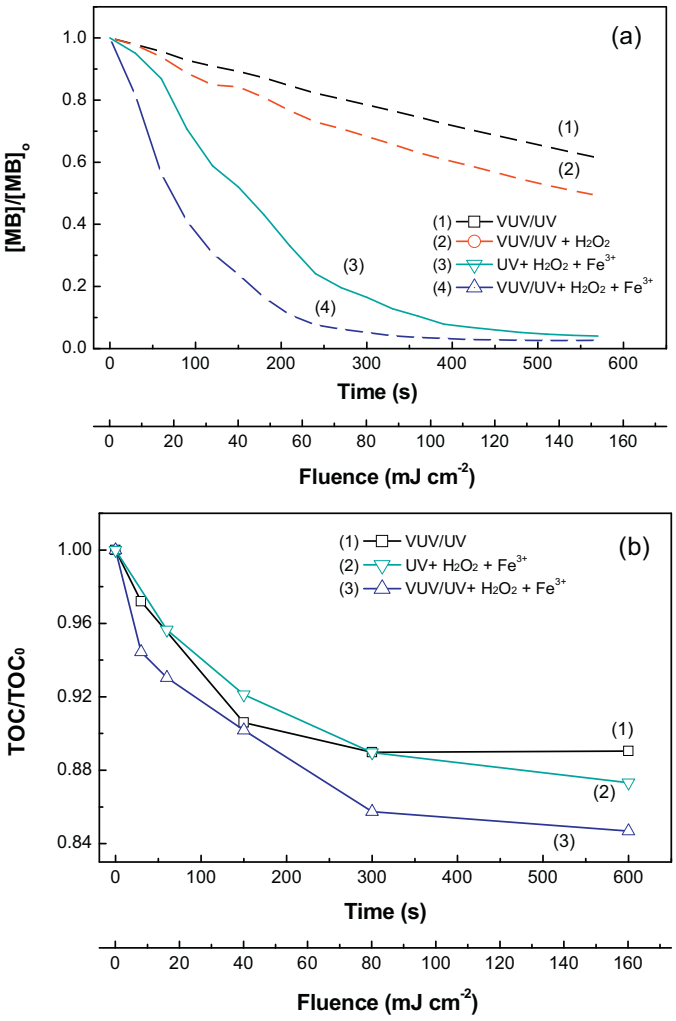

Fig. 2. Methylene blue (MB) degradation (a) and TOC reduction (b) in different photo-Fenton processes. Conditions: $[MB]_0 = 0.016$ mM, $[H_2O_2]_0 = 0.147$ mM, $[Fe^{3+}]_0 = 0.05$ mM, and pH_0 3.3. (For interpretation of the references to colour in this figure legend, the reader is referred to the web version of this article.)

reported in Fig. 2a have been carried out in the presence of air (O_2). The $Fe(III)OH(H_2O)_5^{2+}$ reacts with the O_2 in the photo-reactor leading to $O_2^{-\bullet}$ radicals enhancing further MB degradation since O_2 has been shown to be favorable [46,47] to Fenton/Photo-Fenton reactions.

Fig. 2b presents the mineralization of the MB under different experimental conditions up to 10 min. It is readily seen that the MB-mineralization to CO_2 attains only ~15% after 10 min. This suggests that the MB degradation (Fig. 2a) lead mainly to long-lived intermediates. These results agree with results reported earlier by Herrmann during the photocatalytic discoloration of MB on TiO_2 [48].

3.2. Effects of the solution components on the kinetics of MB degradation: mechanistic considerations

3.2.1. MB degradation induced by VUV/UV and UV light

Fig. 3a shows the MB degradation as a function of the initial dye concentrations from 0.0031 to 0.062 mM. The results demonstrate that high concentrations of MB slow down the degradation kinetics, due to the competition for the limited number of oxidative radicals in solution. MB degradation will also be induced by the direct photolysis by light at 185/254 nm as shown previously in Fig. 2a. Table 1 shows that in the reaction solution ($[MB]_0 = 0.016$ mM,

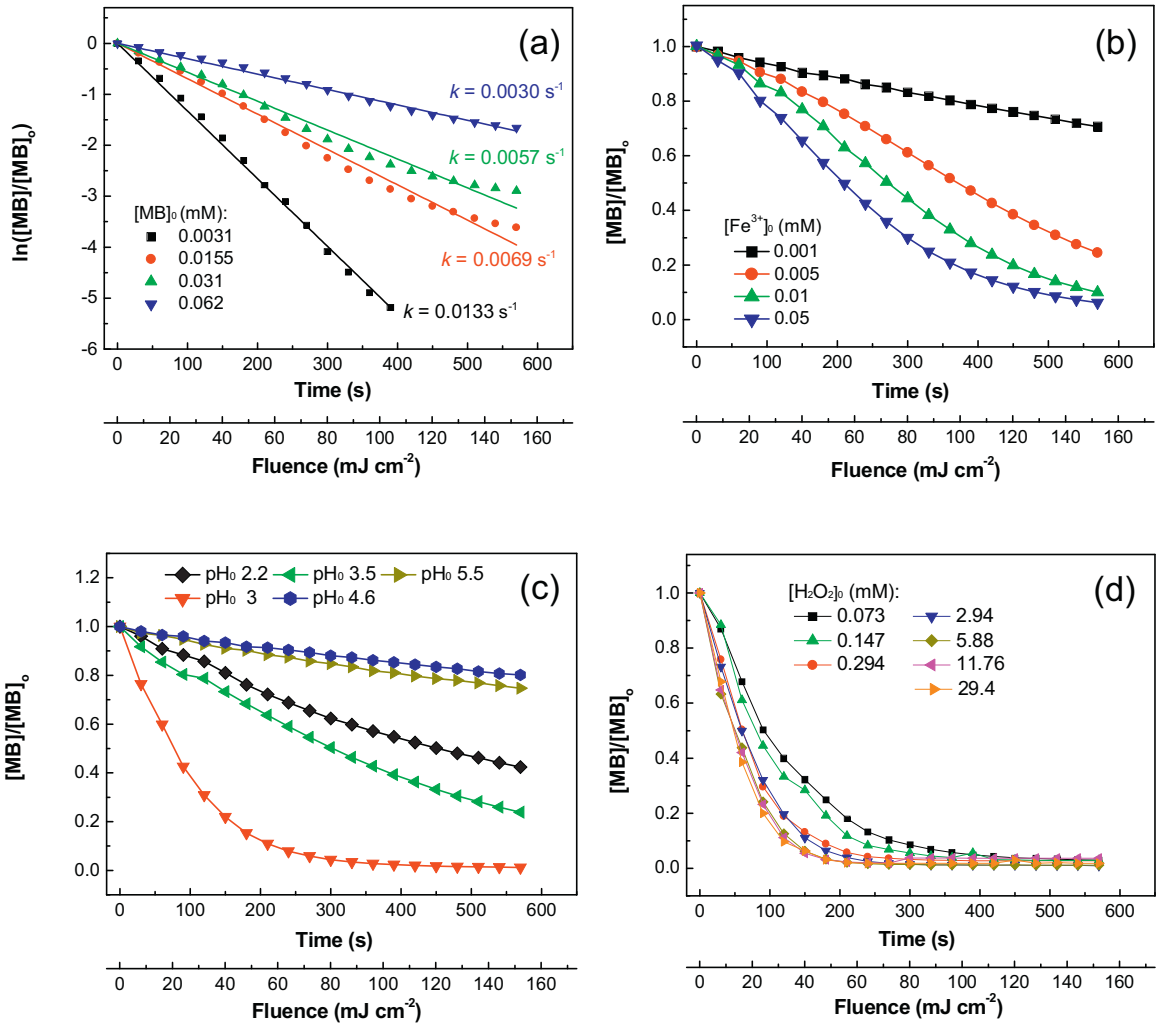

Fig. 3. Effects of the initial concentrations of MB (a), Fe^{3+} (b) and H_2O_2 (c), and the initial pH (d) on MB degradation. (a) MB 0.0031 mM (k 0.0138); MB 0.0155 mM (k 0.069); MB mM 0.031 (0.0057); MB mM 0.062 (0.0030).

$[H_2O_2]_0 = 0.147$ mM, $[Fe^{3+}]_0 = 0.05$ mM), the photons absorbed by MB from the 185 nm light amounted to 5% and 29.8% from the 254 nm second resonance line. The overall MB degradation under VUV/UV light involves the redox reaction shown below in Eq. (11). The initial photo-induced MB• formation is followed by its decomposition within short times [4,10,24,50]. For this reason we address in section 3.3 the scavenging of the •OH/HO_2• radicals, to sort out the participation of these highly oxidative radicals during MB degradation.

$$MB + [Fe(III)OH(H_2O)_5^{2+}] + H_2O + O_2 + H^+ + h\nu \rightarrow [MB/>\ldots Fe(II)(H_2O)_6^{2+}] + {}^{\bullet}OH + MB^+ + HO_2^- \quad (11)$$

The MB• excited state has been reported to be a singlet with a lifetime of 358 ps intercrossing subsequently to the triplet state with a lifetime of 4.5 ms [48,49]. A diluted MB aqueous solution contains an O_2 concentration is 0.5×10^{-3} M. The probability of the triplet MB• deactivation has been reported to be 0.04 [50]. The probability for the collision-controlled deactivation of MB• by O_2 has been reported to be 0.53 [50]. The mechanism of the light induced MB degradation has been extensively reported and will not be discussed further in this study [51,52].

3.2.2. *Effect of the Fe-ions optical band absorption added in solution*

The runs reported in Fig. 3b were carried out at pH 3.3. At this pH the short-hand notation of the predominating species is

Table 1
Reactant concentrations, molar absorption coefficients (ε), absorbance (A), and photon distribution percentage (P) at 254 and 185 nm in the VUV/UV micro photo-reactor.

Reactant	C (mM)	ε_{254} (M^{-1} cm^{-1})	ε_{185} (M^{-1} cm^{-1})	A_{254}	A_{185}	P_{254} (%)	P_{185} (%)
H_2O	55.56	0.01	10	0.010	0.360	16.8	78.3
H_2O_2	0.147	19	341	0.001	0.010	0.9	2.2
$FeCl_3$	0.05	3140	7250	0.031	0.073	52.6	15.8
MB	0.016	5562	7229	0.018	0.023	29.8	5.0
Total						100	100

$Fe(III)(OH)^{2+}$ [42]. The complete species is noted as $Fe(H_2O)_5OH^{2+}$. Under light irradiation, this complex undergoes redox reactions leading to •OH-radicals [11,53,54]:

$$Fe(III)(OH)^{2+} + h\nu \rightarrow Fe(II) + {}^{\bullet}OH \quad (12)$$

The most favorable MB photo-induced degradation was observed adding a concentration of 0.05 mM Fe^{3+} by Fig. 3b. The addition of Fe^{3+} to the MB-solution lead to a faster MB-degradation kinetics since more radicals are formed when more Fe(III) is present. The enhanced H_2O_2 decomposition has been reported due to the increased concentration of the Fe(III)-OO- species in solution [55,56]. The Supplementary material S4 provides information about the spectra of a 0.016 mM MB solution in the presence and absence of $FeCl_3$. This last reagent was used as the source of Fe-ions during this study. The Cl^- anions have a coordinating ability and will substitute water in the first coordination sphere of $[Fe(III)OH(H_2O)_5{}^{2+}]$ yielding mixed ligand complexes such as $Fe(H_2O)_5Cl^{2+}$ and $Fe(H_2O)_4Cl^{2+}$ [57,58].

3.2.3. *Effect of pH on the aqueous solution under VUV irradiation*

The degradation of MB by VUV photo-Fenton processes at various pH's is shown in Fig. 3c. The kinetics presented in Fig. 3c confirms that the full hydrated Fe^{3+}-ion, $Fe(H_2O)_6{}^{3+}$ is the most active catalytic species leading to the fastest MB degradation. When this aqua-metal complex gets de-protonated at pH < 3, it slows down the MB decomposition kinetics. At pH > 3 due, the formation of hydroxylated Fe-complexes up to pH 4.6 also slow down the MB degradation. At pH ~4.6 the $Fe(OH)_3$ precipitates, and slows down the degradation of MB. But the slow MB-degradation involves hydrated Fe-hydroxide species present on the surface of the $Fe(OH)_3$ precipitate.

3.2.4. *Effect of the added H_2O_2 concentration*

The MB degradation kinetics in Fig. 3d is shown to be almost insensitive to the concentration of H_2O_2 added in solution. The MB degradation rate increased slightly upon H_2O_2 addition from 0.073 to 5.88 mM under VUV in a solution with an initial pH 3.3. At H_2O_2 concentrations between the 5.88 and 29.4 mM, the MB degradation was seen to be independent of the added H_2O_2. The excessive H_2O_2 added in solutionscavenged the •OH radical in solution [4,5]. During photo-Fenton reactions, the oxidation of Fe^{2+} to Fe^{3+} with a concomitant evolution of O_2 has been reported [21]. Eq. (13) shows the redox processes in which H_2O_2 is oxidized to O_2 trough a FeO^{2+} intermediate, occurs concomitantly with the FeO^{2+} species reacting with Fe^{2+} reducing H_2O_2 to OH^-

$$Fe^{2+} + H_2O_2 \rightleftharpoons (Fe^{2+}{\cdot}H_2O_2) \xrightarrow{-H_2O} FeO^{2+} \begin{cases} \xrightarrow{H_2O_2} Fe^{2+} + O_2 + H_2O \\ \xrightarrow{Fe^{2+}} 2Fe^{3+} + 2OH^- \end{cases} \quad (13)$$

3.3. *Scavenging of the main species leading to MB degradation*

Fig. 4a shows the MB degradation for a solution by adding various concentration of *tert*-butanol (TBA). A reaction rate of 1.9×109 has been reported for the reaction of TBA with the •OH-radicals as determined by competition kinetics [37,44]. Fig. 4a shows that an increasing the concentration of TBA from 1 mM to 10 mM, led to a MB degradation decreased due to the quenching of the •OH radicals by TBA [4,10,19].

Fig. 4b reports the MB-degradation in solution in the presence of benzoquinone (BQ), a well-known superoxide radical quencher via fast electron transfer [59–61]. Fig. 4b shows that the degradation of MB was completely inhibited by 1 mM BQ. This shows the most active species intervening in MB degradation is HO_2•. BQ scavenges the HO_2• radicals with a bimolecular rate of $9.6 \times 10^8\ M^{-1}s^{-1}$ leading to the formation of O_2 noted below in Eq. (14) [61]:

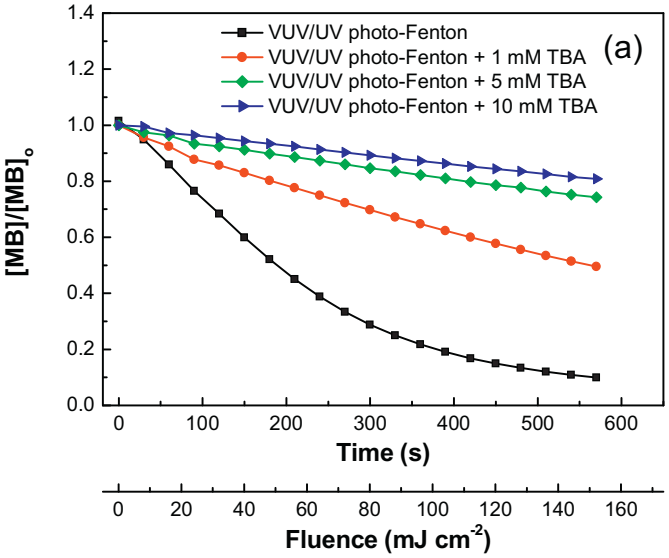

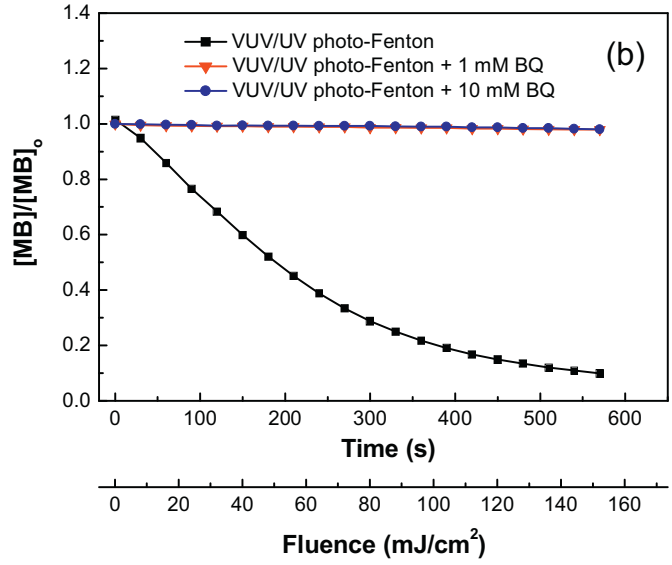

Fig. 4. MB degradation in the presence and absence of *tert*-butanol (TBA) (a) and benzoquinone (BQ) (b) under VUV/UV light irradiation. Conditions: $[MB]_0 = 0.016$ mM, $[H_2O_2]_0 = 0.147$ mM, $[Fe^{3+}]_0 = 0.05$ mM, and $pH_0 = 3.3$.

$$BQ + HO_2{}^{\bullet} \rightarrow BQ^{-\bullet} + H^+ + O_2 \quad (14)$$

The HO_2• radicals disproportionate at pH > 4.8 as shown in Eq. (15):

$$HO_2{}^{\bullet} \Leftrightarrow H^+ + O_2{}^{-\bullet} pK_a = 4.8 \quad (15)$$

Estimation of the •OH radical lifetime takes into account the rate of the reaction $Fe^{2+} + H_2O_2 \rightarrow Fe^{3+} + OH^- + {}^{\bullet}OH$ ($k_1 = 40$–$60\ M^{-1}\ s^{-1}$) and also of the reaction of •OH + MB (RH) → products ($k_2 \sim 10^{10}\ M^{-1}s^{-1}$). Inserting the solution parameters MB = 0.016 mM, $H_2O_2 = 0.147$ mM, $Fe^{3+} = 0.05$ mM in the quasi-stationary state for •OH concentration and approximating the radical concentration to zero (since it is almost negligible), renders a lifetime for the •OH radical ~ 2 ns (see Supplementary material S4).

To estimate the HO_2• radical lifetime, the Eqs: $Fe^{2+} + HO_2{}^{\bullet} \rightarrow Fe^{3+} + HO_2{}^{-\bullet}$, $k_3 = 8 \times 10^5\ M^{-1}\ s^{-1}$ [15] and $HO_2{}^{\bullet} + RH\ (MB) \rightarrow$ product $k_4 \sim 1.2 \times 10^6\ M^{-1}\ s^{-1}$ were considered

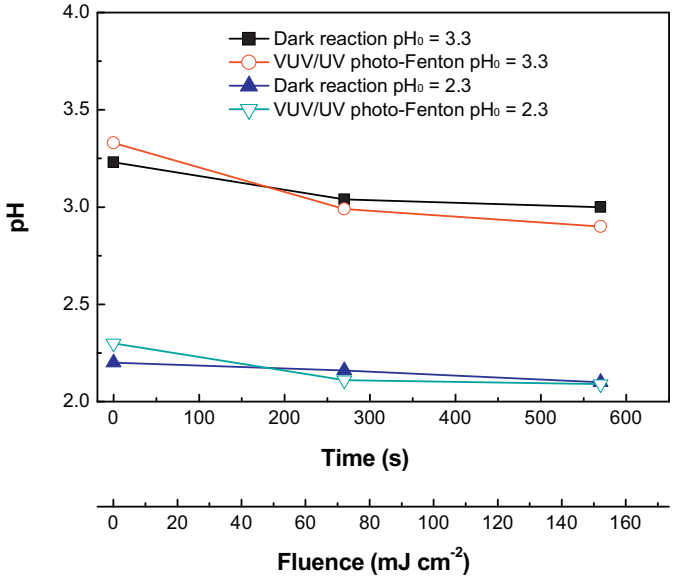

Fig. 5. pH variations during the VUV/UV photo-Fenton and dark-Fenton processes at initial pH values of 2.3 and 3.3. Conditions: $[MB]_0 = 0.016$ mM, $[H_2O_2]_0 = 0.147$ mM, $[Fe^{3+}]_0 = 0.05$ mM.

and allows to estimate a lifetime of 0.38 s for the $HO_2^{\bullet}$ radical. The OH/OH− potential 1.90 eV [62] is higher than the potential of $\cdot HO_2/HO_2^-$ of 0.75 eV [63–65]. The Smoluchowski simplified approximation was used to calculate the mean-free path of the $^{\bullet}OH$, $x_2 \cong D_T$ where D is the diffusion of molecules with a low molecular weight and T is the inverse of the pair MB + $^{\bullet}OH$ lifetime. Inserting the inverse of the reaction rate $10^{10}\ M^{-1}s^{-1}$ and the MB concentration (i.e., 0.016×10^{-3} M) a mean-free path x ≅ 52 nm can be estimated for $^{\bullet}OH$. By the same approach, a mean-free path for the $HO_2^{\bullet}$ radicals of about 580 μ was estimated (see S6). The data in Fig. 4a and b, to suggest that the MB degradation is not controlled by the radical redox-potentials but by the radical lifetimes and mean-free diffusion distances.

3.4. PH shift and pH dependent intervention of the $HO_2^{\bullet}$ radical during MB degradation

Fig. 5 shows that for a solution ([MB] = 0.016 mM, $[H_2O_2]$ = 0.147 mM, [Fe3 +] = 0.05 mM, at an initial pH = 3.3, the pH moves to more acidic values in the dark and under VUV/UV irradiation during MB degradation as suggested in Eq. (16). The pH shift in the solution under VUV/UV from 3.3 to 2.8 shown in Fig. 5 corresponds to a fourfold increase in the H^+ concentration in solution. This pH shift is due to: (a) the MB^+ acid-cation generation noted in Eq. (11), and (b) the build up of short carboxylic long-lived acid intermediates in solution containing COOH groups with pK_a values ~3.0 as reported by Herrmann et al. [48]. The shift to more acid values during the MB-degradation time is suggested in Eq. (16)

(16) $MB^{\bullet} + Fe^{3+} + H_2O \rightarrow MB\text{-}OH + H^+ + Fe^{2+}$

Fig. 6 shows MB degradation by VUV/UV/H_2O_2 (H_2O_2 0.147 mM) process in the presence and absence of BQ at pH values of 3.3 and 5.4. In the dark (full points) BQ did not preclude MB-degradation since no radicals were produced. This is not surprising due to the fact that the oxidation of organic compounds by H_2O_2 in the dark have been reported to be independent of pH [66,67]. But under VUV/UV light, the H_2O_2 at pH 3.3 leads to $HO_2\cdot$ In this case Fig. 6 shows that only about 12% MB was degraded within 10 min. The data at pH 5.4 for light activated MB-degradation shows that no MB degradation was observed at this pH. The reason for this

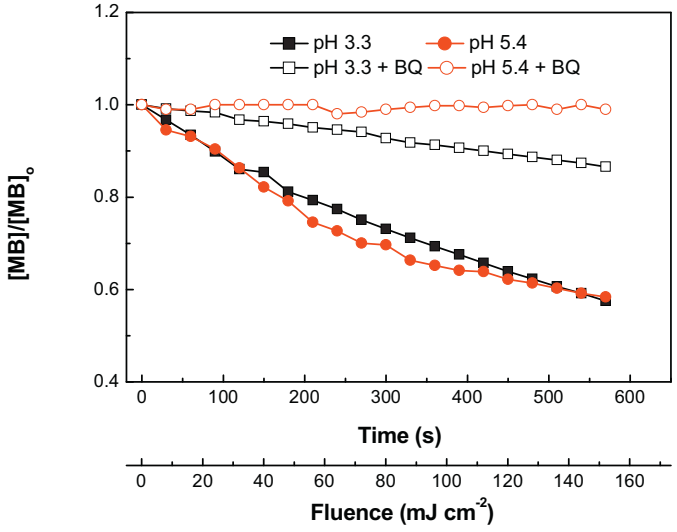

Fig. 6. MB degradation by VUV/UV/H_2O_2 in the presence and absence of BQ at initial pH values of 3.3 and 5.4. Conditions: $[MB]_0 = 0.016$ mM, $[H_2O_2]_0 = 0.147$ mM.

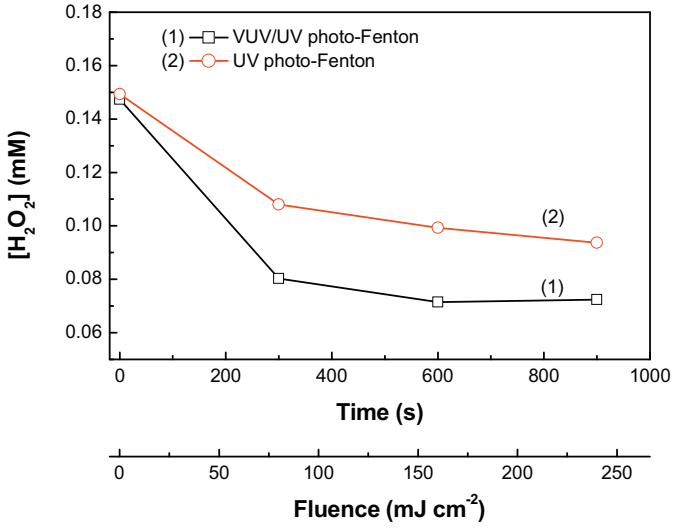

Fig. 7. Change of H_2O_2 concentration with reaction time during the VUV/UV and UV photo-Fenton processes. Conditions: $[MB]_0 = 0.016$ mM, $[H_2O_2]_0 = 0.147$ mM, $[Fe^{3+}]_0 = 0.05$ mM, and pH_0 3.3.

observation is that at pH 5.4, the $HO_2\cdot$ radicals disproportionate to $O_2^{-\bullet}$ as shown previously in Eq. (15).

3.5. H_2O_2 consumption during MB degradation as a function of the applied light

Fig. 7 shows the decrease of the initial concentration of H_2O_2 during VUV/UV photo-Fenton and UV photo-Fenton processes. The former shows a more rapid decrease of H_2O_2 concentration, due to the higher light dose. The H_2O_2 decrease in UV photo-Fenton process is slower when applying only 254 nm light because the molar absorption coefficient of H_2O_2 at 254 nm $19\ M^{-1}cm^{-1}$ is low and the fluence is also not high ($300\ mJ\ cm^{-2}$).

Generation of H_2O_2 during VUV/UV photolysis has been reported in the presence of dissolved O_2 and organic compounds in solution [30,34,35]. The mechanism involves $H^{\bullet}$ trapping by O_2 yielding $HO_2^{\bullet}$. These radicals subsequently recombine to yield H_2O_2. About 0.025 mM H_2O_2 was generated in pure H_2O under VUV/UV (see Supplementary material S7). However, during the MB

degradation by VUV/UV photo-Fenton the amount of H_2O_2 generated by VUV/UV is much lower compared to the added initial H_2O_2 concentration of 0.147 mM.

4. Conclusions

The discoloration/degradation of MB by the Fenton reagent was enhanced by VUV/UV and UV irradiation from low-pressure mercury lamps. The effects of the initial MB, Fe^{3+} and H_2O_2 concentrations were evaluated as well as the effect of the initial pH during the MB degradation. The effect of the HO_2-radical scavenging at different pH and their effect on the MB degradation kinetics was discussed. Appropriate radical scavengers identified the main oxidative radicals leading to MB degradation. The radical lifetimes and their diffusion distances in aqueous solution were estimated. A simplified mechanism for the radical species leading to MB oxidation is suggested in this study.

Acknowledgments

This work was supported by: the National Natural Science Foundation of China (51408592) and Marie Curie/E.U. Seventh Program FP7/2007-2013 under the REA (Agreement No. 318926), the EPFL and COST MP1106.

Appendix A. Supplementary data

Supplementary data associated with this article can be found, in the online version, at http://dx.doi.org/10.1016/j.apcatb.2016.01.014.

References

[1] P. Vandevivere, R. Blanch, W. Verstratete, J. Chem Technol. Biotechnol. 72 (1988) 289–302.
[2] P. Gogate, A. Pandt, Adv. Environ. Res. 8 (2004) 501–551.
[3] T. Openlaender, Photochemical Purification of Water and Air, Wiley-VCH, Weinheim, Germany, 2003.
[4] A. Sychev, Russ. Chem. Rev. 64 (1995) 1105–1129.
[5] Chemical Water Treatment, Principles and Practice, in: H. Roques (Ed.), VCH Publishers Inc., New York 10010, NY, 1995.
[6] Y. Lee, L. Kovalova, C. McArdell, U. von Gunten, Water Res. 64 (2014) 134–148.
[7] N. Cheremisinoff, Handbook of Water and Wastewater Treatment Technologies, Elsevier Inc., 2002, 2016.
[8] Meng Chong, Bo Jin, Christopher Chow, Chris Saint, Water Res. 44 (2010) 2997–3027.
[9] S. Malato, P. Fernandez-Ibanez, I. Maldonado, J. Blanco, W. Gernjak, Catal. Today 147 (2009) 1–59.
[10] J. Schneider, M. Matsuoka, M. Takeuchi, J.L. Zhang, Yu Horiuchi, M. Anpo, D. Bahnemann, Chem. Rev. 114 (2014) 9919–9986.
[11] R. Bauer, G. Waldner, H. Fallmann, S. Hager, M. Klare, T. Krutzler, S. Malato, P. Maletzky, Catal. Today 53 (1999) 131–144.
[12] R. Bauer, H. Fallmann, Res. Chem. Intermed. 23 (1997) 341–354.
[13] N. De la Cruz, L. Esquius, D. Grandjean, A. Magnet, A. Tungler, L.F. de Alencastro, C. Pulgarin, Water Res. 47 (2013) 5836–5845.
[14] D. Spuhler, J.-A. Rengifo-Herrera, C. Pulgarin, Appl. Catal. B: Environ. 96 (2010) 126–141.
[15] J. Kiwi, A. Lopez, V. Nadtochenko, Environ. Sci. Technol. 34 (2000) 2162–2168.
[16] S. Parra, I. Guasaquillo, O. Enea, J. Kiwi J. Phys. Chem. B 107 (2003) 7026–7035.
[17] V. Nadtochenko, J. Kiwi Inorg. Chem. 37 (1998) 5233–5238.
[18] J. Fernandez, J. Bandara, A. Lopez, Ph. Buffat, J. Kiwi, Langmuir 15 (1999) 185–192.
[19] P. MacFaul, D. Wayner, K.U. Ingold, Acc. Chem. Res. 31 (1998) 159–162.
[20] C. Walling, J. Am. Chem. Soc. 8 (1975) 125–130.
[21] M. Kremer, J. Phys. Chem. A. 107 (2003) 1734–1741.
[22] R. Chen, J. Pignatello, Environ. Sci. Technol. 31 (1997) 2399–2406.
[23] J.R. Bolton, C.E. Cotton, The Ultraviolet Disinfection Handbook, 1st edition, American Works Assoc, Denver Colorado, 2008.
[24] E. Legrini, E. Oliveiros, A.M. Braun, Chem. Rev. 93 (1993) 671–684.
[25] K. Zoschke, H. Bornick, E. Worch, Water Res. 52 (2014) 131–145.
[26] A. Bozzi, T. Yuranova, J. Kiwi, J. Photochem. Photobiol. A 172 (2005) 27–34.
[27] T. Oppenlaender, Chem. Eng. Technol. 21 (1998) 502–505.
[28] M. Gonzales, E. Oliveiros, E. Woerner, A.M. Braun, J. Photochem. Photobiol. C 5 (2004) 225–246.
[29] N. Quici, M. Litter, A.M. Braun, E. Oliveiros, J. Photochem. Photobiol. A 197 (2008) 306–312.
[30] G. Imoberdorf, M. Mohseni, Chem. Eng. Sci. 66 (2011) 1159–1167.
[31] M. Satuf, R. Brandi, A.E. Cassano, O.M. Alfano, Appl. Cat. B. 82 (2008) 37–49.
[32] H. Glaze, Y. Lay, W. Kang, Indust. Chem. Eng. Res. 34 (1995) 2314–2323.
[33] J. Crittenden, S. Hu, W. Hand, A. Green, Water Res. 33 (1999) 2315–2328.
[34] S. Robl, M. Worner, D. Maier, A.M. Braun, Photochem. Photobiol. Sci. 11 (2012) 1041–1050.
[35] M. Bagheri, M. Mohseni, J. Hazard. Mater. 294 (2015) 1–8.
[36] P. Ciesla, P. Kocot, P. Mytiych, S. Stasicka, J. Mol. Catal. A 234 (2004) 17–33.
[37] M.K. Li, Z.M. Qiang, T.G. Li, J.R. Bolton, C.L. Liu, Environ. Sci. Technol. 45 (2011) 3034–3039.
[38] C. Duca, G. Imoberdorf, M. Mohseni, Photochem. Photobiol. 90 (2014) 238–240.
[39] D. Wang, T. Oppenlander, M.G. El-Din, J.R. Bolton, Photochem. Photobiol. 86 (2010) 176–181.
[40] N. Klamerth, S. Malato, A. Aguera, A. Fernandez-Alba, G. Mailhot, Environ. Sci. Technol. 46 (2012) 2885–2892.
[41] S. Jin, A. Mofidi, K.G. Linden, J. Environ. Eng. ASCE 132 (2006) 831–841.
[42] A. Safarzadeh, J.R. Bolton, S.R. Carter, J. Adv. Oxid. Technol. 1 (1996) 18–21.
[43] W. Feng, D. Nansheng, Chemosphere 41 (2000) 1137–1147.
[44] Y. Zuo, J. Hoigné, J. Environ. Sci. Technol. 26 (1992) 1014–1019.
[45] S. Bossmann, E. Oliveiros, S. Gob, S. Siegwart, E. Dahlen, L. Straub, M. Worner, A.M. Braun, J. Phys. Chem. 102 (1998) 5542–5551.
[46] B.M. Woelker, F.M. Morel, B. Sulzberger, Environ. Sci. Technol. 31 (1997) 1004–1010.
[47] R. Helz, G. Zepp, G. Crosby, Aquatic and Surface Chemistry, Lewis Pub, Boca Raton, Florida, 1994.
[48] A. Houas, H. Lachheb, M. Ksibi, E. Elaloui, C. Guillard, J.M. Herrmann, Appl. Catal. B 31 (2001) 145–157.
[49] P.V. Kamat, Chem. Rev. 93 (2011) 267–300.
[50] S. Rtimi, C. Pulgarin, R. Sanjines, J. Kiwi, Appl. Catal. B 162 (2015) 236–244.
[51] A. Mills, J. Wang, J. Photochem. Photobiol. A 127 (1999) 123–134.
[52] A. Mills, Appl. Catal. B 128 (2012) 9144–9149.
[53] B.C. Faust, J. Hoigné, Atmos. Environ. 24A (1990) 79–89.
[54] J.H. Baxendale, J. Magee, J. Trans. Faraday Soc. 51 (1955) 205–212.
[55] D.T. Sawyer, C. Kang, A. Llobet, C. Redman, J. Am. Chem. Soc. 115 (1993) 5817–5818.
[56] H. Gallard, J. de Laat, Water Res. 34 (2000) 3107–3116.
[57] V. Balzani, V. Carassiti, Photochemistry of Coordination Compounds, Academic Press, London/NewYork, 1970 (145192).
[58] H. Balkenberg, P. Warneck, J. Phys. Chem. 99 (1995) 5214–5221.
[59] P. Piccinini, C. Minero, M. Vincentini, E. Pelizzetti, J. Chem. Soc. Faraday Trans. 93 (1997) 1993–2000.
[60] P. Wardman, J. Phys. Chem. Ref. Data 18 (1989) 1637–1755.
[61] R. Battino, L. Clever, Chem. Rev. 66 (1966) 395–413.
[62] M.D. Stanbury, Adv. Inorg. Chem. 33 (1989) 69–76.
[63] D. Dophin, B. James, Inorganic chemistry: towards the 21st century, ACS Symp. Ser. 211 (1982) 103–112.
[64] J.H. Merz, W.A. Waters, J. Chem. Soc. (1949) 2427–2434.
[65] L.M. Dorfman, G.E. Adams, Reactivity of the OH-Radical in Aqueous Solutions, Report No NDRDS-NBS-46US Government Washington D.C. 1973.
[66] F. Haber, J. Weiss, Proc. R. Soc. 134 (1934) 332–351.
[67] D. Wang, J.R. Bolton, R. Hofmann, Water Res. 46 (2012) 4677–4686.